Smart Structures and Systems, *Vol. 20, No. 5 (2017) 563-572*
DOI: https://doi.org/10.12989/sss.2017.20.5.563

Vision-based multipoint measurement systems for structural in-plane and out-of-plane movements including twisting rotation

Jong-Han Lee[1a], Chi-Young Jung[*2], Eunsoo Choi[3b] and Jin-Hwan Cheung[4c]

[1]Department of Civil Engineering, Daegu University, Gyeongsan 38453, Republic of Korea
[2]Seismic Simulation Test Center, Pusan National University, Yangsan 50612, Republic of Korea
[3]Department of Civil Engineering, Hongik University, Seoul 04066, Republic of Korea
[4]Department of Civil Engineering, Pusan National University, Busan 46241, Republic of Korea

(Received April 20, 2017, Revised July 25, 2017, Accepted August 9, 2017)

Abstract. The safety of structures is closely associated with the structural out-of-plane behavior. In particular, long and slender beam structures have been increasingly used in the design and construction. Therefore, an evaluation of the lateral and torsional behavior of a structure is important for the safety of the structure during construction as well as under service conditions. The current contact measurement method using displacement meters cannot measure independent movements directly and also requires caution when installing the displacement meters. Therefore, in this study, a vision-based system was used to measure the in-plane and out-of-plane displacements of a structure. The image processing algorithm was based on reference objects, including multiple targets in Lab color space. The captured targets were synchronized using a load indicator connected wirelessly to a data logger system in the server. A laboratory beam test was carried out to compare the displacements and rotation obtained from the proposed vision-based measurement system with those from the current measurement method using string potentiometers. The test results showed that the proposed vision-based measurement system could be applied successfully and easily to evaluating both the in-plane and out-of-plane movements of a beam including twisting rotation.

Keywords: vision; displacement; in-plane; out-of-plane; twisting

1. Introduction

The safety of structures mainly depends on the lateral and twisting behavior as well as the vertical displacement. Recently, long and slender beam structures have been increasingly used in design and construction with the development of high-strength materials and constructional technologies, but there has been increasing concern regarding the lateral behavior and stability of the structures (Brett and Lu 2013, Han *et al*. 2015, Lee *et al*. 2017, Patrick 2016). Therefore, an evaluation of the lateral and torsional behavior of a structure is important for the safety of the structure during construction as well as the performance of the structure under service conditions. Analytical investigations into the safety of structures have focused on the classical stability theory, which is limited to the critical load related to the lateral and torsional instability. Therefore, several studies (Darılmaz 2011, Li *et al*. 2002, Shirazizadeh *et al*. 2016, We *et al*. 2014, Xue and Chen 2015, Lee 2017) employed the finite element method to account for the nonlinear properties of material, geometry, and boundary conditions in the lateral and torsional behavior of structures. Several researchers (Hurff and Kahn 2012, Kalkan 2014, Lee 2012a, Lee 2012b, Lee and Kalkan 2012) have examined the influence of lateral deformation on the safety of bridge girders. The safety of the structure is closely associated with the lateral deformation of the structure. Moreover, out-of-plane lateral deformation includes in-plane vertical deformation and twisting rotation of the structure.

To evaluate the in-plane and out-of-plane behavior of a structure, the displacements are commonly measured using displacement meters, such as LVDT (linear variable differential transformer) and string potentiometers. However, these contact methods cannot directly measure the vertical and lateral displacements. Indeed, the vertical and lateral displacements are combined with a twisting rotation. That is, the displacements and rotation cannot be obtained directly from the values measured from the displacement meters. In general, the coupled displacements are analyzed using the method developed by Zhao *et al*. (1994, 1995) and modified by Stoddard (1997), Kalkan and Hurff (2012), and Lee *et al*. (2017). The current method to calculate the independent lateral and vertical displacements and twisting angle assumes that each string potentiometer comprises a right-angle triangle between the object, reference point, and wire. This assumption requires

∗Corresponding author, Research Professor
E-mail: cyjung@pusan.ac.kr
[a] Assistant Professor
E-mail: jonghan@daegu.ac.kr
[b] Professor
E-mail: eunsoochoi@hongik.ac.kr
[c] Professor
E-mail: cheung@pusan.ac.kr

http://www.techno-press.com/journals/sss&subpage=7
ISSN: 1738-1584 (Print), 1738-1991 (Online)

particular care to maintain perfectly horizontal and vertical lines of the wires between the potentiometers and structure in three-dimensional space.

Therefore, a noncontact vision-based measurement system is used to evaluate the in-plane and out-of-plane movements including the twisting angle. The vision-based measurement system has been applied effectively to measure the displacements in the fields of civil and architectural engineering (Feng and Feng 2016, Fukuda *et al*. 2013, Lee *et al*. 2012, Lin *et al*. 2015, Ye *et al*. 2013, Ye *et al*. 2016). The image processing algorithm involved in this study is based on the color information of several reference objects in Lab color space. To increase the accuracy of the area of multiple targets from the entire image, a flood fill algorithm with eight directions was used to recognize the boundary of the target regions. To synchronize the time of the captured targets and a main server, this study used a load indicator wirelessly connected to a data logger system in the server. In the post-processing step, the displacements and rotation of a structure were calculated at the targets, which could be located in the top or bottom of the structure due to the condition of the installation. Then, the coordinates of the centroid of the section were used to obtain the relationship between the load and vertical displacement, and the load and lateral displacement. The proposed vision-based measurement system was verified using a laboratory beam test. The test results showed that the in-plane and out-of-plane displacements including a twisting rotation obtained from the proposed vision-based measurement system matched well with those from the current measurement method using string potentiometers.

2. Development of vision-based measurement system

2.1 Current measurement method

The structure of a beam mainly supports vertical loads, which has attracted attention to the vertical movement of the flexural member. In addition to the vertical in-plane movement, the safety of the structure is mainly associated with the out-of-plane movement. In particular, slender and long structural members have been increasingly used with the development of high-strength materials and construction technologies. Such slender and long members are more vulnerable to the out-of-plane movement. The in-plane and out-of-plane movements of a structure are combined with twisting rotation. Therefore, a method that can measure the independent displacements and rotation is required.

The current method to obtain the vertical and lateral movements and rotational angle from the coupled deflections is based on the measurement technique using three potentiometers proposed originally by Zhao *et al*. (1994, 1995) and later expanded by Stoddard (1997). The method was recently expanded by Kalkan and Hurff (2012) and Lee *et al*. (2017). Fig. 1 illustrates the configuration of the measurement method using three potentiometers for a rectangular beam. Two lateral potentiometers, denoted as A and B, are connected to the top and bottom edges of the section, and one vertical potentiometer, denoted as C, is placed under the beam and connected to the bottom edge of the section. As the beam begins to deform, the initial string lengths of those potentiometers vary with the coupled deflections, as shown in Fig. 1. As a first step, the vertical and lateral deflections at a point of the beam, B_x and B_y, respectively, to which the lateral and vertical potentiometers are connected, are calculated using the following equations based on the assumed two right-angled triangles

$$(B_o - B_x)^2 + B_y^2 = B_f^2 \tag{1}$$

$$(C_o - B_y)^2 + B_x^2 = C_f^2 \tag{2}$$

where B_o and C_o are the initial string lengths of the bottom and vertical potential meters, respectively, and B_f and C_f, are the changed string lengths of the bottom and vertical potential meters, respectively. Solving Eqs. (1) and (2) give the following two sets of solutions

$$(B_x, B_y) = \left(\frac{K_p + C_0 L_p}{N_p}, \frac{M_p + B_0 L_p}{N_p} \right) \tag{3}$$

$$(B_x, B_y) = \left(\frac{K_p - C_0 L_p}{N_p}, \frac{M_p - B_0 L_p}{N_p} \right) \tag{4}$$

where

$$K_p = B_o^3 - B_o B_f^2 + B_o C_o^2 + B_o C_f^2 \tag{5}$$

$$M_p = C_o^3 - C_o C_f^2 + C_o B_o^2 + C_o B_f^2 \tag{6}$$

$$L_p = \sqrt{\begin{matrix} -B_o^4 - B_f^4 + 2B_o^2 B_f^2 + 2B_o^2 C_f^2 + 2B_f^2 C_f^2 \\ -C_o^4 - C_f^4 + 2C_o^2 C_f^2 - 2B_o^2 C_o^2 + 2B_f^2 C_o^2 \end{matrix}} \tag{7}$$

$$N_p = 2(B_o^2 + C_o^2) \tag{8}$$

Among the two solutions, Eqs. (3) and (4), one solution should be selected and compared with the real behavior of the structure. After determining one realistic solution, the twisting angle of the beam section is calculated using another right-angled triangle assumed at the top lateral potentiometer. Therefore, the following equation can be obtained using the Pythagorean theorem

$$[B_o - B_x - h \cdot \sin\phi]^2 + [B_y + h \cdot (\cos\phi_i - \cos\phi)]^2 = A_f^2 \tag{9}$$

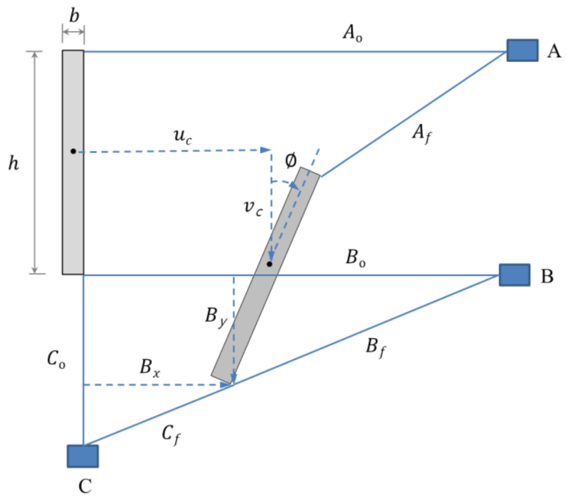

Fig. 1 Configuration of the current measurement method using the potentiometers

where h is the depth of the beam, ϕ_i is the initial rotational angle, and A_f is the changed string length of the top lateral potentiometer. The twisting angle of a beam, ϕ, obtained from Eq. (9), also produces two solutions, which means that one realistic solution should be selected.

Finally, after determining the twisting angle of the beam, the lateral and vertical deflections at the centroid of the beam section, u_c and v_c, respectively, are calculated using the following equations, which have been derived from the deformed geometry.

$$u_c = B_x + \frac{h}{2}(\sin\phi - \sin\phi_i) + \frac{b}{2}(\cos\phi_i - \cos\phi) \tag{10}$$

$$v_c = B_y + \frac{h}{2}(\cos\phi_i - \cos\phi) - \frac{b}{2}(\sin\phi - \sin\phi_i) \tag{11}$$

where b is the width of the beam.

The current measurement method assumes that the three potentiometers, physically connected to the beam section in the lateral and vertical directions, comprise a right-angle triangle at the connection of each potentiometer. In fact, the assumption on the right-angle triangles requires special care and attention at the installation of the potentiometers in three-dimensional space. In addition, a series of calculations are carried out to determine the lateral and vertical displacements and twisting angle from the coupled measurements. Furthermore, the displacements and rotations obtained from the current method need to be selected for an appropriate solution by comparing the solutions with the real behavior of the structure.

2.2 Vision-based system and image processing algorithm

For easy and accurate measurements of the in-plane and out-of-plane movements including a twisting angle, this study proposes vision-based measurement method that calculates the movement of targets attached to an object. In general, a method of recognizing a target in the image processing converts the target image captured in color to those in grayscale. The grayscale image is converted to a binary image that has only true and false colors (or, white and black colors, respectively) based on an arbitrary threshold. The image processing algorithm using the binary image has the advantage of analyzing multiple targets located in an image using a single and simple operation. On the other hand, the true and false colors in the binary image are strongly dependent on the value of a certain threshold, which should be defined by the users. Fig. 2 presents the binary images of a target converted from an original image with the change in the threshold value. The size and location of the target can differ significantly according to the value of the threshold, which means that a trial and error method is required to obtain an optimal result.

Therefore, in this study, color information was used to distinguish the area of multiple targets from the entire image. Fig. 3 shows the algorithm of the image processing method used in this study. The algorithm using the color information of the reference targets consists of four steps; 1) an image acquisition step to capture the image, 2) an image processing step to identify the color information of the image, 3) an image analysis step to recognize the targets on the image and synchronize the time of the target with that of the external load, and 4) a post-processing step to determine the in-plane and out-of-plane deformations.

The accuracy of measurement is determined by the resolution of the images obtained in the image acquisition step. Therefore, a digital camera that is more cost-effective and higher in resolution than a digital camcorder is used to achieve the target images. The image processing step is then carried out to identify the color information of the captured image. The colors of the several reference objects, including the targets, specimen, and background, are extracted to evaluate the color throughout the entire image per unit pixel. The area identified as the target in the image is

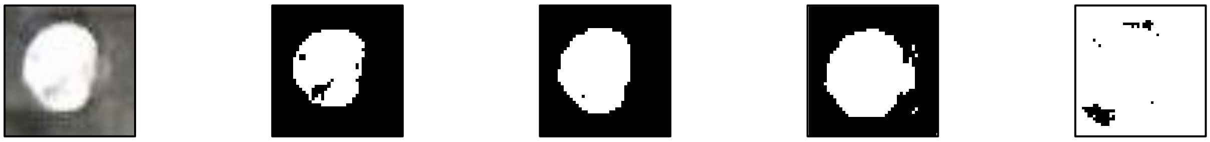

(a) (b) (c) (d) (e)

Fig. 2 Binary images obtained from the image processing with a threshold value (TH); (a) original image, (b) TH=0.9, (c) TH=0.75, (d) TH=0.5, and (e) TH==0.25

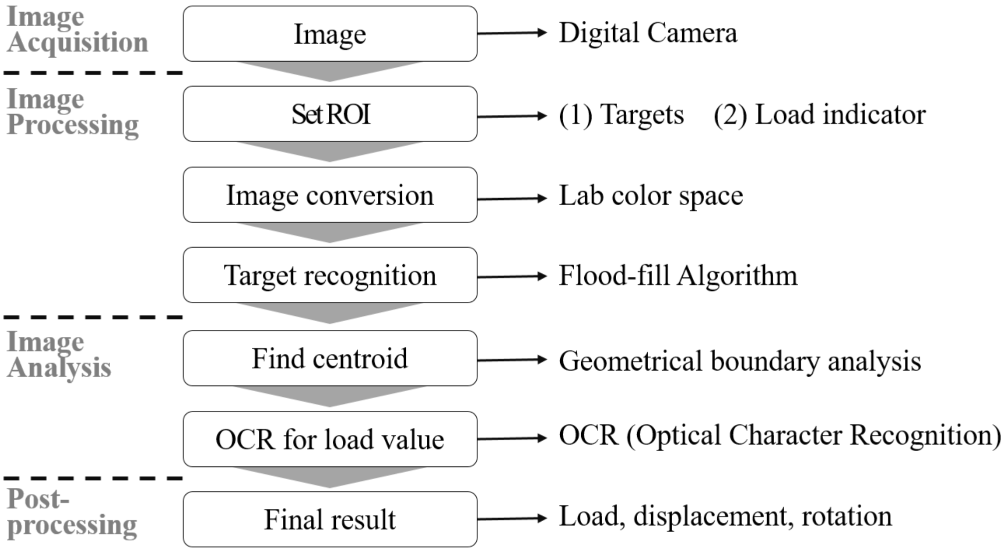

Fig. 3 Algorithm for measuring the load and displacements using an image processing method

(a) (b)

Fig. 4 Color spaces; (a) Lab color space and (b) RGB color space

converted to the binary image and is represented by a number of one as the true value. To accurately evaluate the color information in the image, the Lab color space was used instead of the commonly-used RGB color space. This is because the Lab color space can distinguish more clearly the difference in contrast in the same chroma than the RGB color space (Kaur and Kranti 2012) and accurately find the region, which matches with the color of the target. Fig. 4 shows the difference between the Lab and RGB color spaces. In the Lab color space, the color information is evaluated based on the distance (D_{ij}) between the reference colors and the color at a pixel i location using the following Eq. (12).

$$D_{ij} = \sum_{j=1}^{n}\sum_{i=1}^{m}\left(\sqrt{(L_j - L_i)^2 + (a_j - a_i)^2 + (b_j - b_i)^2}\right) \tag{12}$$

where L_i, a_i, and b_i represent the color information at the location of a pixel i, and L_j, a_j, and b_j represent the color information of a reference j, as shown in Fig. 4. When D_{ij} becomes zero, the corresponding pixel is determined to be the reference target.

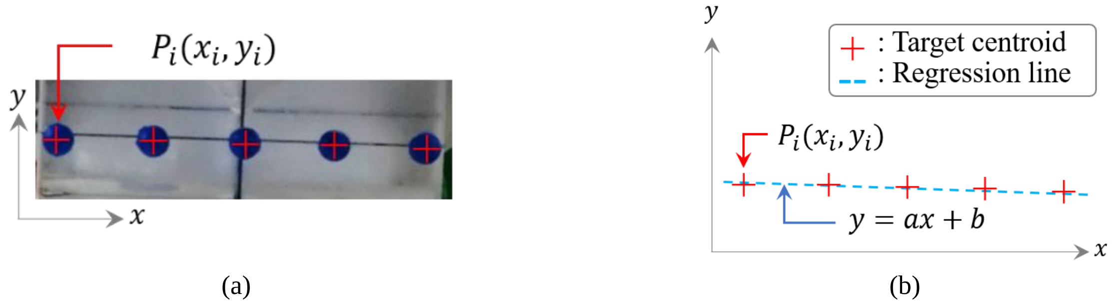

Fig. 5 Calculation of the slope and displacement of the targets; (a) centroid of the targets and (b) coordinates and regression line of the target centroids

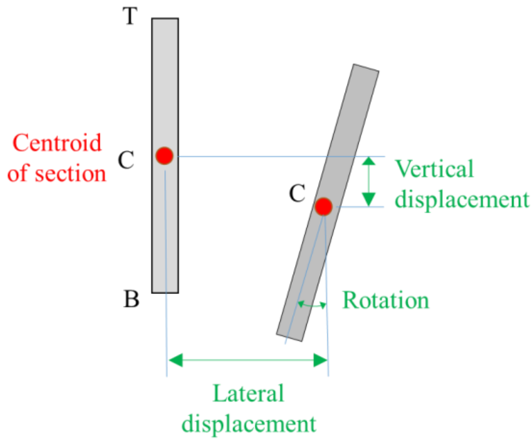

Fig. 6 Vertical and lateral displacements and twisting rotation at the center of a cross- section

In the image analysis step, the flood-fill algorithm was used to recognize the boundary of the target area defined in the image processing step. The recursive flood fill algorithm with eight directions was used to increase the recognition rate of the boundary of the target region (Ye *et al*. 2016). The centroid of each target was calculated by analyzing the sectional properties of the boundary including the target area. Then, the coordinates of the target per each frame can be calculated. Using the coordinates of the targets, linear regression analysis was carried out to calculate the initial slope and displacements in the member and the difference of the slope and displacements between the frames of an image, as shown in Fig. 5. The load value, which is displaced on the indicator, was quantified by the OCR (Optical Character Recognition) algorithm (Smith *et al*. 2009). This process was repeated to determine the vertical and lateral displacements and twisting rotation of the structure synchronized with the load value.

The design and analysis of structures normally focus on the deformations at the centroid. Therefore, in the post-processing step, the vertical and lateral displacements and twisting rotation at the centroid of the structure is calculated assuming the rigid body motion of the cross-section. Because twisting rotation occurs with respect to the center of the section, rotation has no influence on the vertical and lateral displacements at the centroid. Therefore, the displacements and rotation at the center of the cross-section can be calculated using the following procedure. As an example of a structure with a rectangular section shown in Fig. 6, the twisting rotation and vertical and lateral displacements are first calculated at the targets located in the either top or bottom of the structure (points T and B, respectively, in Fig. 6). The coordinates of the centroid of the section (point C) are then calculated from a reference point of the target. Finally, the determined coordinates of the centroid are used to obtain the relationship between the load and vertical displacement, and the load and lateral displacement.

3. Experimental program

3.1 Laboratory test

The proposed vision-based measurement system was verified using a laboratory beam test. The test beam was defined as a doubly-symmetric I-shape that has commonly been applied to design and construction in the field. Based on the small-sized beam tests performed by Lee *et al*. (2017), the shape and material of the test specimen were determined for the laboratory test. The total height of the beam was 72 mm, and the width and thickness of the top and bottom flanges were 40 mm and 6 mm, respectively.

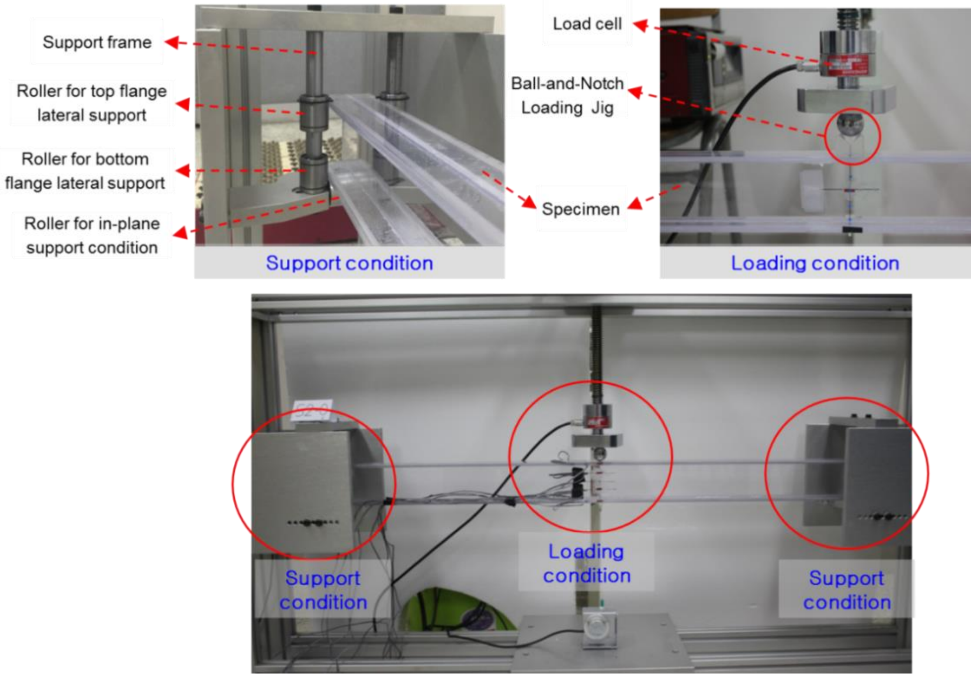

Fig. 7 Installation of the specimen

The length of the beam was defined as 1000 mm. The specimen was manufactured using polycarbonate with the advantage of its linear elasticity; the modulus of elasticity of polycarbonate is 2400 N/mm^2, and the yield strength is 52 N/mm^2 (Shah *et al*. 2005). The specimen defined in this study has a width-to-thickness ratio of 3.3 for the top and bottom flanges and 10 for the web members, which did not show any local buckling problem during the test.

3.2 Specimen setup and instrumentation

The specimen was installed on a simply-supported condition. The span length of the beam specimen between the supports was 950 mm. The simply-supported condition, which was implemented using a roller, restrains the vertical and lateral translations but allows in-plane flexural behavior of the beam (or, the flexure in the strong axis). When the lateral and twisting rotation (out-of-plane) movements occur, the beam could be unstable, leading to sudden failure of the beam. Therefore, to maintain the lateral stability of the beam, lateral support was provided to restrain the lateral transition and twisting rotation at the location of the in-plane simply-supported condition at both ends but allow the out-of-plane flexural behavior of the beam (or, the flexure in the weak axis). Fig. 7 presents the beam specimen installed on both the in-plane and out-of-plane support conditions. The ball casters at the top and bottom flanges of the beam, shown in Fig. 7, provide a lateral support condition to the top and bottom flanges of the beam, to restrain the lateral translational movement at the support locations. A vertical point load was then applied to the middle of the top surface of the beam, and the magnitude of the load was measured using a load cell installed in the vertical loading system.

The in-plane and out-of-plane displacements and twisting rotation at the mid-span were determined using the vision-based measurement system proposed in this study. The measurement system could have some interruptions, such as difficulties in access, obstructions to installation, and traffic conditions. Therefore, the vision-based measurement system needs to be installed in the top or bottom of the structure. Considering the measurement conditions, the vision-based measurement systems were carried out for three cases: Case 1 using the targets installed on the top surface of the specimen, case 2 using the targets on the corner edge of the top part of the specimen, and case 3 using the targets installed on the corner edge of the bottom part of the specimen. Fig. 8 presents the proposed vision measurement system and the targets installed at the specimen. For case 1, blue-color targets were attached on the top surface of the specimen. For case 2, red and green colors were attached to the left and right corners of the top of the specimen, respectively. Finally, for case 3, where the installation of the vision-based system is required in the bottom of a structure, similar to case 2, green and red colors were attached to the both corners of the bottom part of the specimen. In addition to the targets, an indicator connected wirelessly to a main server is captured to synchronize the time of the target image and server. In this study, the magnitude of the load in a data logger system is used as an indicator to synchronize the load and displacements, obtained from the cameras. That is, a captured image includes both the displacements of the targets and the load indicator. The cameras used in this study were SONY Alpha 7R, which has its own automatic function to correct for image distortion depending on the lens specifications of the camera. The resolution of the image was 7360 pixels in width and 4912 pixels in height; hence, the image has a

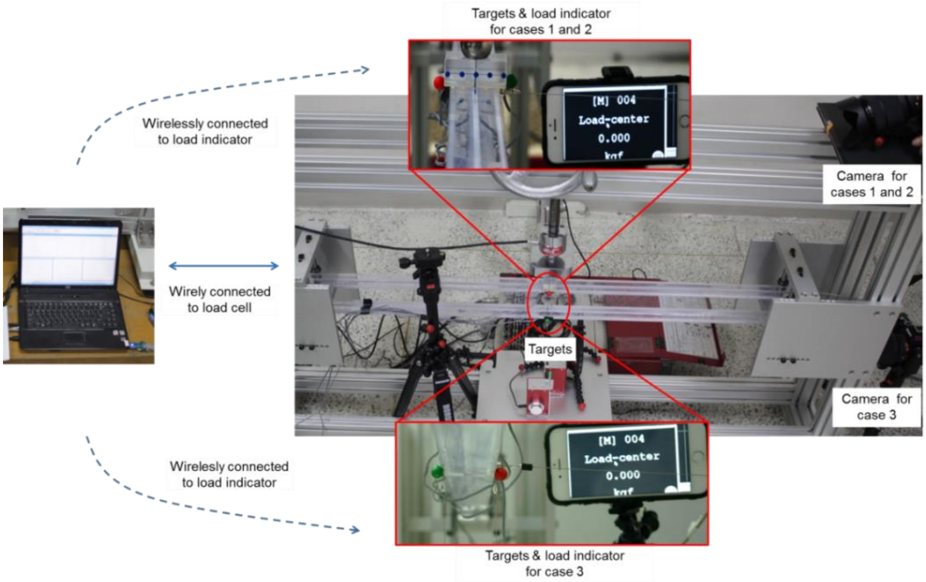

Fig. 8 Experimental setup for the vision-based measurement system

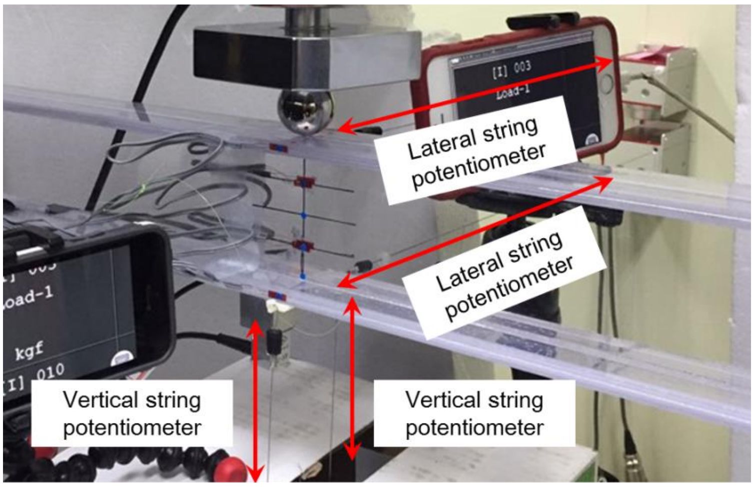

Fig. 9 String potentiometers installed at the mid-span

total of 36 million pixels. The measurement resolution obtained from the image processing is approximately 0.08mm similar to that from a 100mm linear variable differential transformer (LVDT). The images were automatically acquired at an interval of 1 second.

For comparison with the proposed vision-based measurement system, the current method using string potentiometers was used to measure the displacements and twisting of the beam at the mid-span, as shown in Fig. 9. Because the displacements are combined with the twisting of the beam, the measurement technique described in Section 2.1 should be used to acquire the independent displacement components, lateral and vertical displacements and twisting rotation. Therefore, a total of three string potentiometers were installed: Two horizontal potentiometers at the top and bottom flanges of the beam and one vertical potentiometer at the location of the bottom flange.

4. Results and discussions

The in-plane and out-of-plane displacements and twisting angle measured from the proposed vision-based system were compared with those obtained from the current measurement method using string potentiometers. Figs. 10 to 12 show the vertical and lateral displacements and twisting angles at the shear center (or centroid) of the cross-section at the mid-span of the beam specimen. As the vertical load, which mainly governs the in-plane vertical movement, increases, the lateral displacement and twisting angle also increase the likelihood of lateral instability of the beam. In particular, the twisting angle rapidly increases with increasing load, as shown in Fig. 12. Therefore, when the lateral displacement and twisting angle were approximately 2 mm and 3°, respectively, the load was stopped to prevent sudden lateral collapse of the beam. The proposed vision-based measurement system showed good

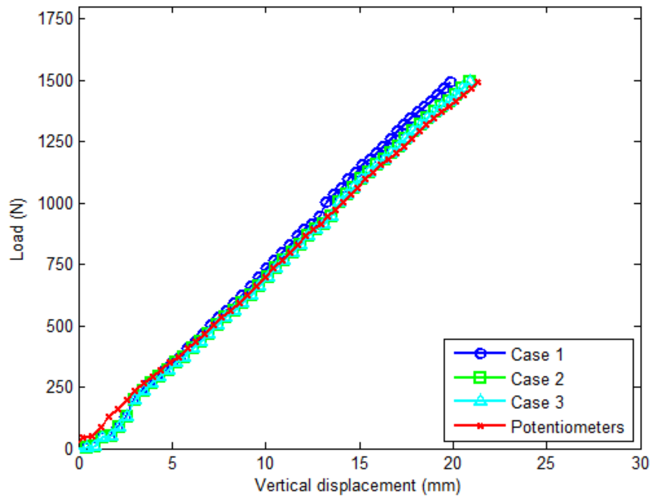

Fig. 10 Load and vertical displacement curves measured from the proposed vision-based system and potentiometers

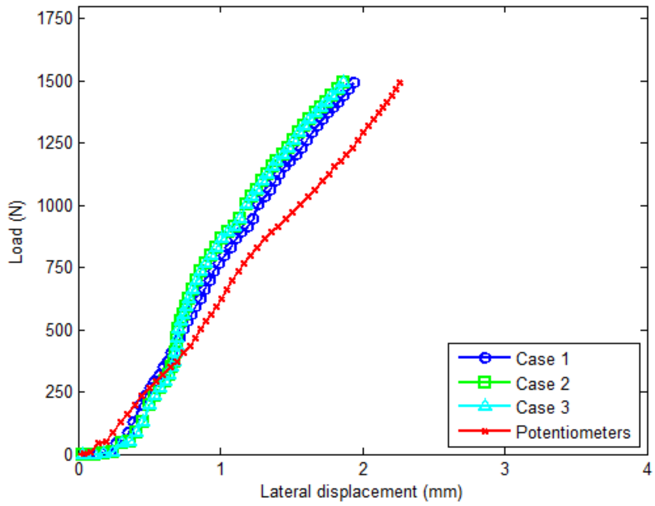

Fig. 11 Load and lateral displacement curves obtained from the string potentiometers and proposed vision-based system

agreement with the measurement method using potentiometers, which require a particular caution in the instrumentation and a series of calculation to determine the independent displacements from the measured coupled displacements. The lateral displacement and twisting angle in the small range of the response, shown in Figs. 10 and 12, respectively, show some differences between the vision-based system and contact method. This might be due to the string potentiometers, which assume right-angles at the connections of the specimen, potentiometer, and reference point.

Error analysis was performed using the root mean squared error (RMSE) to quantify the difference between the measurements obtained from the proposed vision-based system and those from the current measurement method using potentiometers, as follows

$$\mathrm{RMSE} = \sqrt{\frac{\sum_{i=1}^{n}(x_i - y_i)^2}{n}} \tag{13}$$

where n is the number of the measurement data, and x_i and y_i are the displacement components measured from the vision-based system and current contact method, respectively.

Table 1 lists the RMSE errors of the displacements and twisting angles for the three cases: Case 1 using targets on the top surface, case 2 using targets on the corner edge of the top part, and case 3 using targets on the corner edge of the bottom part. The vision-based system demonstrated high measurement accuracy for the in-plane vertical and out-of-plane lateral movements including the twisting angle with a

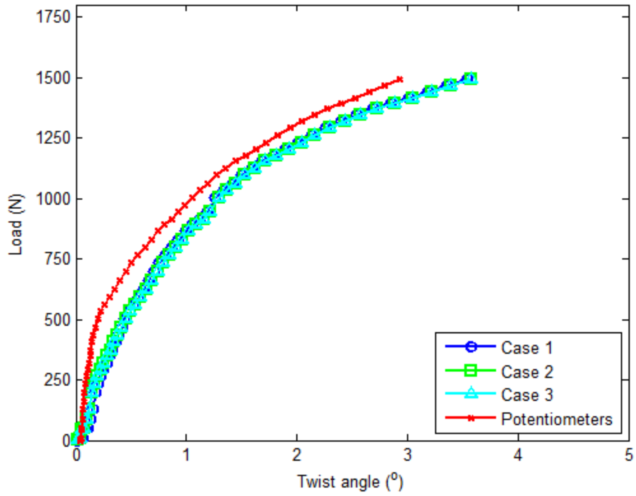

Fig. 12 Load and twisting angle curves obtained from the string potentiometers and proposed vision-based system

Table 1 Errors of the vision-based measurement system and contact measurement method

Components	RMSEs of the vision-based measurements		
	Case 1	Case 2	Case 3
Vertical displacement (mm)	0.558	0.690	0.660
Lateral displacement (mm)	0.186	0.255	0.127
Twisting angle (°)	0.427	0.448	0.481

maximum RMSE error of 0.690 mm, 0.255 mm, and 0.487°, respectively. The measurements were similar in all three cases. Therefore, the proposed vision-based system can allow flexibility regarding the measurement locations for monitoring the in-plane and out-of-plane movements of a structure. Furthermore, the proposed vision system can synchronize the movements along with the change in load applied to the structure, which facilitate measurements and evaluations of the structural performance according to the applied load.

5. Conclusions

Recently, long and slender beam structures have been increasingly used in the design and construction with the development of high-strength materials and constructional technologies, but there has been increasing concern regarding the lateral behavior and stability of the structures. Therefore, an evaluation of the lateral and torsional behavior of a structure is important for the safety of the structure during construction as well as the performance of the structure under service conditions. The current measurement method using displacement meters cannot measure the vertical and lateral displacements directly. Therefore, a series of calculations and particular caution regarding instrumentation are required to determine the independent displacements from the couple measurements with a twisting angle. Furthermore, the displacements and twisting angle calculated from the current method should be selected to obtain an appropriate solution by comparing the solutions with the real behavior of the structure.

A vision-based measurement system was proposed to acquire the independent in-plane and out-of-plane movements including the twisting angle of a structure. The image processing algorithm involved in this study was based on several reference objects, including multiple targets in Lab color space. The proposed vision-based measurement system was verified using a laboratory beam test. The in-plane and out-of-plane displacements including twisting rotation obtained from the proposed vision-based measurement system showed a good match with those from the current measurement method using string potentiometers. As a result, the proposed vision-based system can overcome the limitations of the current method, such as instrumentation of the displacement meters, analysis of the coupled measurements, and selection of an appropriate solution. Furthermore, the proposed vision-based system allows flexibility in installation to account for some interruptions and expand the measurement points and targets to determine the independent displacements and twisting rotation. In addition, a technology using the wireless load indicator can synchronize the times between the targets and match the movements of the structure and load applied externally to the structure.

Acknowledgements

"This research was supported by a grant (17CTAP-C132963-01) from Technology Advancement Research Program funded by the Ministry of Land, Infrastructure and Transport (MOLIT) of Korea government and Korea Agency for Infrastructure Technology Advancement (KAIA)."

References

AISC (American Institute of Steel Construction) (2005), *Steel construction manual*, American Institute of Steel Construction, Chicago, IL, USA.

Brett, C. and Lu, Y. (2013), "Assessment of robustness of structures: Current state of research", *Front. Struct. Civil Eng.*, **7**(4), 356-368.

Darılmaz, K. (2011), "An assumed stress hybrid finite element for buckling analysis", *Math. Comput. Appl.*, **16**(2), 690-701.

Feng, D. and Feng, M.Q. (2016), "Vision-based multipoint displacement for structural health monitoring", *Struct. Control Health Monit.*, **23**, 876-890.

Fukuda, Y., Feng, M.Q., Narita, Y., Kaneko, S. and Tanaka, T. (2013), "Vision-based displacement sensor for monitoring dynamic response using robust object search algorithm", *IEEE Sens. J.*, **13**(12), 4725-4732.

Han, Q., Liu, M., Lu, Y. and Wang, C. (2015), "Progressive collapse analysis of large-span reticulated domes", *Int. J. Steel Struct.*, **15**(2), 261-269.

Hurff, J.B. and Kahn, L.F. (2012), "Lateral-torsional buckling of structural concrete beams: experimental and analytical study", *ASCE J. Struct. Eng.*, **138**(9), 1138-1148.

Kalkan, I. (2014), "Lateral torsional buckling of rectangular reinforced concrete beams", *ACI Struct. J.*, **111**(1), 71-81.

Kalkan, I. and Hurff, J.B. (2012), "Experimental techniques for lateral stability testing of beams", *Exp. Techniques*, **39**(5), 36-47.

Kaur, A. and Kranti, B.V. (2012), "Comparison between YCbCr color space and CIE Lab Color space for skin color segmentation", *Int. J. Appl. Inform. Syst.*, **3**(4), 30-33.

Lee, J.H. (2012a), "Behavior of precast prestressed concrete bridge girders involving thermal effects and initial imperfections during construction", *Eng. Struct.*, **42**, 1-8.

Lee, J.H. (2012b), "Investigation of extreme environmental conditions and design thermal gradients during construction for prestressed concrete bridge girders", *ASCE J. Bridge Eng.*, **17**(3), 547-556.

Lee, J.H. (2017), "Evaluation of the lateral stability of precast beams on an elastic bearing support with a consideration of the initial sweep", *Eng. Struct.*, **143**, 102-112.

Lee, J.H. and Kalkan, I. (2012), "Analysis of thermal environmental effects on precast, prestressed concrete bridge girders: temperature differentials and thermal deformations", *Adv. Struct. Eng.*, **15**(3), 447-459.

Lee, J.H., Ho, H.N., Shinozuka, M. and Lee, J.J. (2012), "An advanced vision-based system for real-time displacement measurement of high-rise buildings", *Smart Mater. Struct.*, **21**(12), 125019.

Lee, J.H., Kalkan, I., Lee, J.J. and Cheung, J.H. (2017), "Rollover instability of precast girders subjected to wind load", *Mag. Concrete Res.*, **69**(2), 68-83.

Lee, J.H., Park, Y.M., Jung, C.Y. and Kim, J.B. (2017), "Experimental and measurement methods for the small-scale model testing of lateral and torsional stability", *Int. J. Concrete Struct. Mater.*, **11**(2), 377-389.

Li, J.Z., Hung, K.C. and Cen, Z.Z. (2002), "Shell element of relative degree of freedom and its application on buckling analysis of thin-walled structures", *Thin Wall. Struct.*, **40**, 865-876.

Lin, C.W., Hsu, W.K., Chiou, D.J., Chen, C.W. and Chiang, W.L. (2015), "Smart monitoring system with multi-criteria decision using a feature based computer vision technique", *Smart Struct. Syst.*, **15**(6), 1583-1600.

Patrick, S. (2016), "Structural safety of masonry walls during the work: Considerations from practice", *Structural Analysis of Historical Constructions: Anamnesis, diagnosis, therapy, controls*. CRC Press, London, 1138-1141.

Shah, Q.H., Homma, H., Iliyas, M.H. and Ismail, A.F. (2005), "The effect of material property gradient on the fracture toughness of a PMMA/PC bimaterial with a crack normal to the interface", *J. Appl. Sci.*, **5**, 476-481.

Shirazizadeh, M.R., Shahverdi, H. and Imam, A. (2016), "A simple finite element procedure for free vibration and buckling analysis of cracked beam-like structures", *J. Solid Mech.*, **8**(1), 93-103.

Smith, R., Antonova, D. and Lee, D. (2009), "Adapting the tesseract open source OCR engine for multilingual OCR", *Proceedings of the International Workshop on Multilingual OCR*, Article No. 1.

Stoddard, W.P. (1997), "Lateral-torsional buckling behavior of polymer composite I-shaped members", Ph.D. Dissertation, Georgia Institute of Technology, Atlanta, GA.

Wu, D., Gao, W., Tangaramvong, S. and Tin-Loi, F. (2014), "Robust stability analysis of structures with uncertain parameters using mathematical programming approach", *Int. J. Numer. Meth. Eng.*, **100**(10), 720-745.

Xue, J.F. and Chen, J.F. (2015), "Reinforcement strength reduction in FEM for mechanically stabilized earth structures", *J. Central South Univ.*, **22**(7), 2691-2698.

Ye, X.W., Dong, C.Z. and Liu, T. (2016), "Force monitoring of steel cables using vision-based sensing technology: methodology and experimental verification", *Smart Struct. Syst.*, **18**(3), 585-599.

Ye, X.W., Ni, Y.Q., Wai, T.T., Wong, K.Y., Zhang, X.M. and Xu, F. (2013), "A vision-based system for dynamic displacement measurement of long-span bridges: algorithm and verification", *Smart Struct. Syst.*, **12**(3), 363-379.

Zhao, X.L., Hancock, G.J. and Trahair, N.S. (1994), *Lateral Buckling Tests of Cold-formed RHS Beams*, Research Report R699, School of Civil and Mining Engineering, The University of Sydney, Australia.

Zhao, X.L., Hancock, G.J. and Trahair, N.S. (1995), "Lateral buckling tests of cold-formed RHS beams", *J. Struct. Eng. - ASCE*, **121**(11), 1565-1573.

HJ